

Architecture and protocols for all-photonic quantum repeaters

Naphan Benchasattabuse^{*§}, Michal Hajdušek^{*§}, and Rodney Van Meter^{‡§}

^{*}Graduate School of Media and Governance, Keio University Shonan Fujisawa Campus, Kanagawa, Japan

[‡]Faculty of Environment and Information Studies, Keio University Shonan Fujisawa Campus, Kanagawa, Japan

[§]Quantum Computing Center, Keio University, Kanagawa, Japan

{whit3z,michal,rdv}@sfc.wide.ad.jp

Abstract—An all-photonic repeater scheme based on a type of graph state called a repeater graph state (RGS) promises tolerance to photon losses as well as operational errors, and offers a fast Bell pair generation rate, limited only by the RGS creation time (rather than enforced round-trip waits). Prior research on the topic has focused on the RGS generation and analyzing the secret key sharing rate, but there is a need to extend to use cases such as distributed computation or teleportation as will be used in a general-purpose Quantum Internet. Here, we propose a protocol and architecture that consider how end nodes participate in the connection; the capabilities and responsibilities of each node; the classical communications between nodes; and the Pauli frame correction information per end-to-end Bell pair. We give graphical reasoning on the correctness of the protocol via graph state manipulation rules. We then show that the RGS scheme is well suited to use in a link architecture connecting memory-based repeaters and end nodes for applications beyond secret sharing. Finally, we discuss the practicality of implementing our proposed protocol on quantum network simulators and how it can be integrated into an existing proposed quantum network architecture.

Index Terms—Quantum Networking, Quantum Repeaters, All-photonic Repeaters, Quantum Communication, Quantum Optics, Network Protocols, Graph State

I. INTRODUCTION

Attenuation of optical signals in fiber leads to an exponentially vanishing probability of photon arrival as the distance between network nodes increases, limiting practical quantum communication via direct photon transmission to only a few tens of kilometers. Quantum repeaters [1], [2] are one of the cornerstones to realizing long-distance quantum networks and eventually a global Quantum Internet [3], [4]. An all-photonic quantum repeater based on *repeater graph states* (RGS) [5] is the most recent addition to the various repeater schemes, promising higher repetition rate and intrinsic tolerance to both quantum operational errors and loss errors, and most importantly, does not require quantum memories, unlike traditional quantum repeaters. Despite these attractive features, the majority of related research has been focused solely on metrics based on secret key sharing [6]–[8]. Questions of ending the connection, details of quantum as well as classical communication between various network nodes, or integration

of RGS repeater links into other architectures have gone largely underexplored.

In this work, we present three contributions to the practical implementation of the RGS scheme. We first propose an architecture, including a communication protocol, to address the question of how end nodes should participate in the connection via the RGS repeater link type for teleportation-based applications. Second, by considering the full communication cost that is required to establish an end-to-end correctable Bell pair, we demonstrate that a naive approach does not lead to a scalable architecture and propose a solution using progressive correction by intermediate nodes. Finally, in the spirit of interoperability and heterogeneity of classical networks, we demonstrate that our architecture can be integrated with other memory-based architectures by treating RGS links as virtual physical links.

Unlike the current Internet, the goal of quantum networks is not to simply send and receive data between distant parties. The main objective of quantum networks is to distribute entangled resources among distant parties. These entangled resources can then be consumed to perform various tasks such as sending quantum data via teleportation [9], secret key sharing [10], [11], quantum metrology [12], [13], blind quantum computation [14]–[16], or distributed quantum computation [17]–[19]. This sharing of entangled states can be done both via creating the entangled states locally and then sending the states directly or establishing a generic entangled state, such as a graph state or Bell pairs, which can then be used to perform the aforementioned tasks [20], [21]. Here, we focus on the latter approach and only focus on distributing bipartite maximally entangled states.

We will begin by explaining what a graph state is, its extension to the vertex decorated variant, and how to manipulate them via their visual description, which we will use to reason about the correctness of the protocol (Sec. II). Equipped with the knowledge of the graph state manipulation rules, we will then describe the graph-based all-photonic repeater protocol that uses RGS to distribute Bell pairs (Sec. III). We will then propose an architecture that supports the RGS-link type protocol and how end nodes, which are usually left out of the discussion in most literature, are integrated into the architecture (Sec. IV). Since the graph state can deviate from

This material is based upon work supported by the Air Force Office of Scientific Research under award number FA2386-19-1-4038.

its non-vertex-decorated description upon measurement and upon a special operation called local complementation, we will walk through how to keep track and correct the resulting state into a final Bell pair shared between two end nodes in the connection path (Sec. V). Later, we will talk about the full protocol, which information should be sent to end nodes, and which can remain local. How each of the network components performs its operation in order to finally distribute a correctable Bell pair between two end nodes is described in Sec. VI. Finally, we will discuss the implications and possible extensions of the architecture and the protocol. We also discuss implementation plans for a simulator based on this architecture and our future work on implementing this protocol into our network simulator (QuISP) [22], which already supports key elements of this architecture we propose (Sec. VII).

II. PRELIMINARIES: GRAPH STATE

In this section, we begin with a brief description of graph states and their visual manipulation rules.

A. Graph states

Graph states [23], [24] are a class of quantum states which have an intuitive description in terms of mathematical graphs. A mathematical graph $G = (V, E)$ is a pair of a vertex set $V = \{v_1, v_2, v_3, \dots, v_n\}$ and an edge set $E = \{(u, v) | u, v \in V\}$ with $n = |V|$. Here, we only consider undirected simple graphs where only one edge is allowed between a pair of vertices and there are no self-loops. A useful notion is that of the neighborhood of a vertex a , $N_a = \{v | (a, v) \in E\}$, that is a set of all vertices which are connected by an edge to the vertex a . In the graph state formalism, a vertex represents a qubit while an edge represents an interaction between two qubits. Since the graph has no ordering, that means the interaction via the edge of the graph must commute with all other edge operations. The edge interaction is given by the controlled-phase gate CZ ,

$$CZ = |0\rangle\langle 0| \otimes I + |1\rangle\langle 1| \otimes Z. \quad (1)$$

The graph state can be generated by initializing all qubits in the +1 eigenstate of the Pauli X operator and applying CZ entangling gates between the appropriate qubits,

$$|G(V, E)\rangle = \prod_{(u,v) \in E} CZ(u, v) |+\rangle^{\otimes n}. \quad (2)$$

Graph states are a subclass of more general stabilizer states [25]. They can be described in terms of stabilizer generators,

$$g_i = X_i \bigotimes_{v \in N_i} Z_v, \quad (3)$$

associated with each vertex in V . Qubit i and its neighborhood N_i are called the *support* of the stabilizer generator g_i . The graph state $|G(V, E)\rangle$ is the simultaneous +1 eigenstate of all the stabilizer generators $\{g_1, \dots, g_n\}$. An example of a graph with its corresponding stabilizer generators is depicted in Fig. 1(a).

B. Vertex decorated graph state

Two stabilizer states $|\psi_1\rangle$ and $|\psi_2\rangle$ are said to be *LC* (local Clifford) equivalent if one can be transformed into another via the application of single-qubit Clifford gates,

$$|\psi_1\rangle = \bigotimes_{i=1}^n C_i |\psi_2\rangle, \quad (4)$$

where $C_i \in \mathcal{C}_1$, with \mathcal{C}_1 being the local Clifford group.

Since a graph state is also a stabilizer state, the application of Clifford gates onto a graph state is also a stabilizer state. We make frequent use of the *decorated graph state* introduced in [26],

$$|G; \underline{C}\rangle = |G; C_1, C_2, \dots, C_n\rangle = \bigotimes_{i=1}^n C_i |G\rangle. \quad (5)$$

The Clifford operator acting on each vertex is called a *vertex operation* (VOP), and it has been shown that any stabilizer state can be brought into a decorated graph state representation [27]–[29]. When drawing a decorated graph state, we will put a letter next to the vertex to denote the Clifford operator acting on the graph state. An example of a vertex-decorated graph and its corresponding quantum circuit is shown in Fig. 1(b).

C. Local complementation

One interesting operation that can be applied to the graph state which changes the connectivity of the graph is called *local complementation*. Local complementation of graph G at a , denoted by $L_a G$, is the application of single-qubit gates on the vertex a and its neighborhood N_a ,

$$|L_a G\rangle = U |G\rangle = \sqrt{-iX_a} \prod_{v \in N_a} \sqrt{iZ_v} |G\rangle, \quad (6)$$

and the resulting graph $L_a G$ is transformed by complementing the subgraph of G induced by the neighborhood N_a of a . It is worth mentioning that $U \propto \sqrt{K_a}$, and one could also define local complementation as U^\dagger as well.

When local complementation acts on a decorated graph state $|G; \underline{C}\rangle$, the operator U is applied before the decorated Clifford gates (right applied) as

$$|L_a G; \underline{C}\rangle = \left(\bigotimes_{i=1}^n C_i \right) U |G\rangle. \quad (7)$$

An example of applying local complementation on a decorated vertex graph state is shown in Fig. 1(c).

D. Measurement on graph state

From the definition of a graph state, one could write

$$|G\rangle = \frac{1}{\sqrt{2}} |0\rangle_a \otimes |G - a\rangle + \frac{1}{\sqrt{2}} |1\rangle_a \otimes Z_{N_a} |G - a\rangle, \quad (8)$$

where we abuse the notation by referring to Z_{N_a} as applying Z to all neighbors of a . It then follows directly that measurement in the Z basis removes the vertex a from the graph G without changing any edge structure of the remaining induced

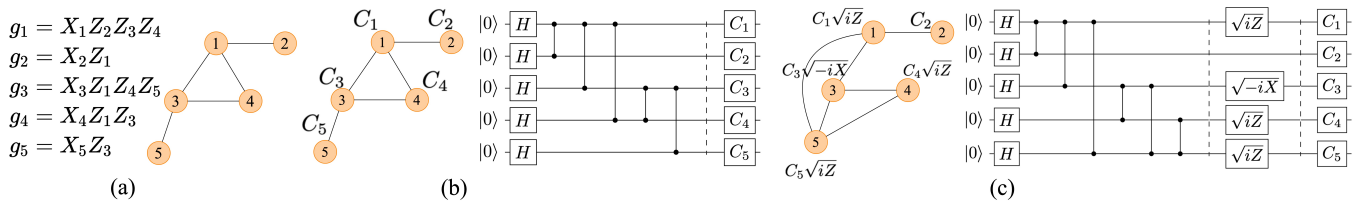


Fig. 1. (a) A graph state example with corresponding stabilizer generators. (b), (c) Vertex decorated graph state and the quantum circuit representation. (b) and (c) are the exact same state achieved by performing local complementation L_3 on vertex 3.

subgraph $G - a$. Neighboring vertices of a are affected by a Pauli Z operator if the -1 eigenvalue is obtained from the measurement as depicted in Fig. 2(a).

Measurements in the X and Y basis can be described as

$$P_{Y,\pm}(a) |G\rangle = P_{Z,\mp}(a) \sqrt{iX_a} |G\rangle, \quad (9)$$

$$P_{X,\pm}(a) |G\rangle = P_{Z,\mp}(a) \sqrt{iX_a} \sqrt{-iZ_a} |G\rangle, \quad (10)$$

where $P_{B,\pm}$ is a measurement in B basis while reporting the results as ± 1 eigenvalue. Note that this is not unique, and there are other possible ways to translate one measurement basis into another one via the addition of Clifford gates. It then follows that we can utilize local complementation to cancel the change of basis Clifford gates on a and perform Z -measurement on the transformed graph. An example of Y -measurement is shown in Fig. 2(b).

Another important measurement sequence that is common in measurement-based quantum computation and also for graph state manipulation is the XX -measurement on two vertices connected via an edge. Suppose the two qubits a and b are measured in this fashion, the resulting graph from the measurement is $G' = G - a - b$, followed by the complementation of the induced subgraph $N_a + N_b$ (graphical derivation is shown in Fig. 2(c)-(d)).

III. ALL-PHOTONIC QUANTUM REPEATER

Graph states can be utilized as resources for various quantum communication tasks including the building of a quantum repeater [5], [30]–[32]. In this section, we review the basics of all-photonic repeaters based on RGS [5].

A. RGS scheme overview

The core principle of the all-photonic repeater, which we will call the RGS scheme from now on, is to utilize a particular highly entangled graph state, as shown in Fig. 3. The RGS comprises $2m$ physical qubits and $2m$ logical qubits forming two sets of qubits; the inner logical qubits, also called first-leaf qubits, which are all connected into a complete graph and the outer arm physical qubits, also called second-leaf qubits. RGS is defined by a parameter m which refers to the number of arms and a branching vector $\vec{b} = (b_1, b_2, \dots, b_n)$ denoting the logical tree encoding of the first-leaf qubits used for counterfactual measurement [33]. These two parameters determine how much loss and error the RGS can tolerate.

Before explaining what these two sets of qubits do, let's consider a connection path between two end nodes. In the RGS

scheme, there are two node types acting as the intermediate nodes: the RGS source (RGSS) and the adaptive measurement node or the advanced Bell state analyzer (ABSA). We follow the node names, icons, and definitions mentioned in [34]. The RGSS's responsibility is to generate the RGS, and send one half to one ABSA and the other half to another partner ABSA, which we refer to as the left and right ABSAs. The ABSA's job is to perform a series of measurements on the incoming half-RGSs from two RGSSs, thus creating a longer distance shared entangled state (Fig. 3).

B. Measurement sequence at ABSA

For simplicity, we assume that each ABSA is holding the two half-RGSs from the two RGSSs and can measure them in any order. Later, we will lift this assumption and describe how to perform the same sequence of measurements in the case of photons being sent one-by-one from the RGSS. We will now outline how adaptive measurements at the ABSA are performed in three stages. For the moment, we will only focus on manipulating the graph structure since in every step the graph structure will be LC-equivalent to what we want and only differ by some VOPs on the qubits. Later in Sec. V, we will discuss how to keep track of and correct these VOPs introduced from each operation.

The first stage is the Bell state measurement (BSM) of second-leaf qubits. In this step, ABSA measures a second-leaf qubit pair in the rotated Bell basis. One qubit of the pair has arrived from the left RGSS and the other qubit from the right one. The rotated BSM can be implemented by first performing a CZ between the two qubits and then measuring both of them in the X basis (recall XX -measurement in Sec. II-D). In Sec. V, we will show that we can perform BSM in the conventional Bell basis as well. Since Bell measurement using linear optics is probabilistic with a maximum success rate of 50%, and photons may get lost in the fiber, we consider failure when the photons are lost or BSM itself fails. These two-qubit measurements are performed on all second-leaf qubits that have arrived at the ABSA.

If *at least one pair of the second-leaf qubits* is successfully measured, we clear the first stage and continue onto the second stage. Recall that measuring a qubit of a graph state in the Z basis is the same as removing that vertex from the graph. We then perform Z -measurements on the first-leaf qubits connected to the second-leaf qubits that failed the BSM. If all the Bell measurements fail in any of the ABSAs along the

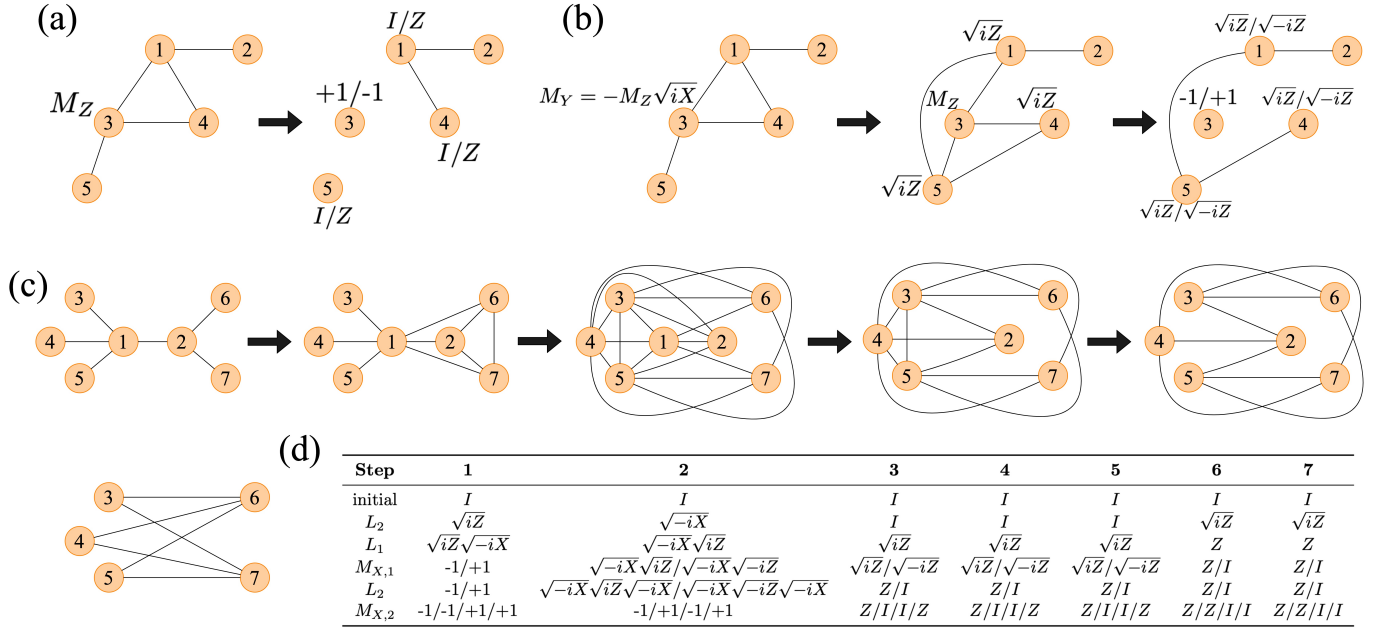


Fig. 2. Visual manipulation of graph state upon measurements. (a) Z basis measurement on vertex 3 of the graph state. (b) Y basis measurement on vertex 3 of the same graph state. Y -measurement is turned into Z -measurement and local complementation is performed to remove the VOP into identity. (c) XX -measurement on two neighbor qubits, the visual derivation is shown in steps, and the VOPs are tracked in table (d).

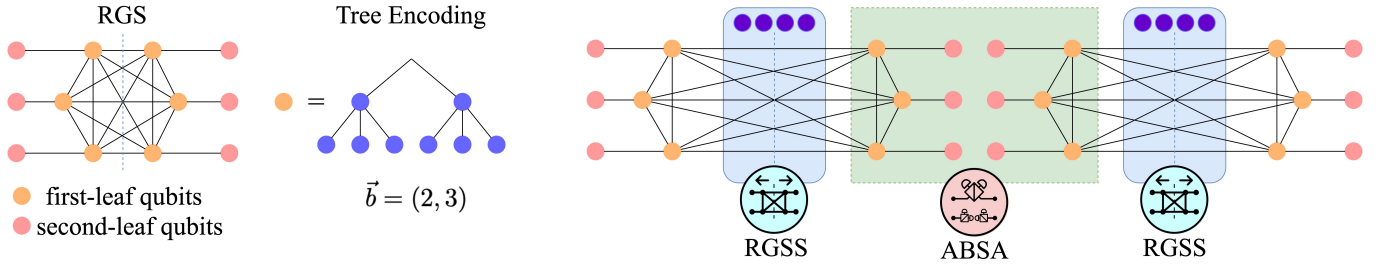


Fig. 3. (left) An example of RGS with parameter $m = 3$ and $\vec{b} = (2, 3)$. First-leaf qubits (orange) are tree-encoded logical qubits while the second-leaf qubits (pink) are physical qubits. Each orange qubit comprises of 8 physical qubits (blue) in this example. (right) RGS source nodes generate RGS and send half to the measurement node, ABSA. (RGSS and ABSA icons are taken from [34])

connection path, then the entire connection trial is a failure and must be attempted again from the beginning. Those first-leaf qubits connected to successfully measured second-leaf qubits are also subjected to Z -measurement except for a single pair of qubits. After all the Z -measurements are performed, the state that we are left with is a linear chain graph state. The process we just described is depicted in Fig. 4.

Finally, all first-leaf qubits in the linear chain are measured in the X basis. Since there are two qubits located in each ABSA at this stage, this is the XX -measurement. The resulting state is a locally equivalent Bell pair shared between the two end nodes. This is the reverse of the traditional quantum repeater schemes where Bell pairs are first created in segments between neighboring repeaters and later spliced into a longer Bell pair via a process called entanglement swapping [35]. Due to this fact, the RGS scheme is considered a time-reversed protocol [36], [37] of the conventional repeater since

entanglement swap is encoded in the RGS first-leaf qubits before the neighbor link level is established from the BSM of second-leaf qubits.

C. Loss tolerance of RGS

From the previous section, it can be seen that one way of battling the loss of photons is to increase the number of arms $2m$, which in turn improves the probability of obtaining at least one successful BSM. However, blindly increasing the number of arms is not the best approach since all the first-leaf qubits need to be successfully measured as well. The analysis of the tradeoff between m and the branching vector \vec{b} is out of scope for this paper and we refer readers to [7], [8].

The second approach to loss tolerance includes encoding the first-leaf qubits and performing logical measurements on them. Since the first-leaf qubits are encoded via tree encoding, the logical measurement can be done via a process called

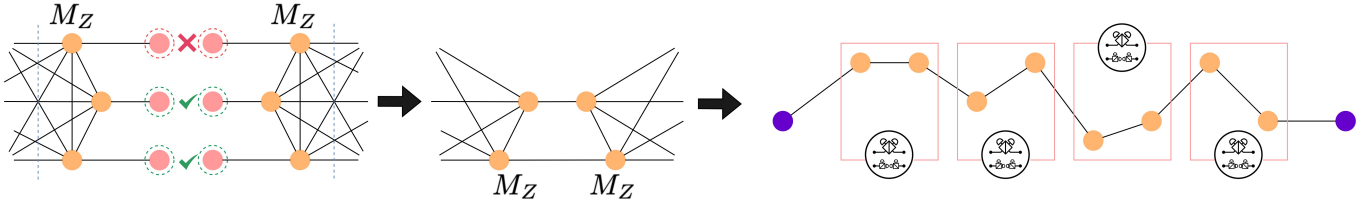


Fig. 4. Steps in realizing RGS scheme at each ABSA; removing first-leaf qubits which connected to failed BSM second-leaf qubits via Z -measurement; removing all but one first-leaf qubits pair that are left. The resulting linear chain of graph state where two first-leaf qubits are located at every ABSA.

counterfactual measurement or *indirect measurement* [33]. The logical measurement is achieved by performing physical qubit measurements on the qubits in different levels of the tree as depicted in Fig. 5. For the X (Z) basis measurement, we perform X (Z) measurement on the first level of the tree and alternate into Z (X) measurement on the second level. The alternation of the basis on the tree level is done for every level, meaning that for X (Z) basis measurement, X (Z) measurement is done on the odd level while Z (X) measurement is done on the even level.

The concept behind the counterfactual measurement comes from the fact that graph states can be described using the stabilizer formalism. The measurement result of qubit a which is part of the support of the stabilizer generator g_i can be deduced if all other qubits in the generator were successfully measured (either directly or indirectly). So the Z -measurement result of a qubit a at level k can be deduced if any of its neighbors b at level $k+1$ are successfully directly measured in the X basis and all of N_b in level $k+2$ are also successfully measured in the Z basis (either directly or indirectly), as shown in Fig 5.

D. Operational error tolerance of RGS

In addition to loss tolerance, RGS also offers tolerance to quantum operation errors. Similar to the loss tolerant capability of the tree encoding, only physical qubits to be measured in the Z basis can be corrected. Correcting a qubit at level k can be achieved by performing a majority vote on the measurement result of the neighbor qubits at level $k+1$ and its neighbors at level $k+1$. This implies that the capacity to tolerate errors of RGS also depends on the loss probability of photons.

IV. ARCHITECTURE

In this section, we turn our attention to the end nodes. Incorporating end nodes into the RGS scheme has not been explored aside from quantum key distribution (QKD) applications where end nodes are merely measurement nodes and not full compute nodes. The main difference in having compute nodes as opposed to measurement nodes is the requirement that compute nodes need to have quantum memories storing the states and wait for all the measurement result messages from ABSA and RGSS to arrive before the Bell pairs are ready for use. One possible way to realize this was explored in [8], where the end nodes must be equipped with at least m quantum memories, and for one trial, having m memories

emit photons to meet with half-RGS at an ABSA. We argue that this approach is inefficient and goes against the core idea of having RGS in the first place. Since the main appeal points of the RGS scheme are the one-way messaging from RGSSs and ABSAs to end nodes which enable the high repetition trial rate and relax the number of quantum memories, to fully utilize these properties of the RGS scheme, end nodes need to have rm memories where r is the time it takes for the classical message to arrive from the furthest ABSA divided by the RGS generation time. A rough calculation shows that end nodes would require ~ 150 memories for 1000 km using the results presented in [7] to keep up with the trial rate ($r = 10$, $m = 15$). Instead, we will show that in our architecture, we only need r quantum memories and m emitters at end nodes ($r + m$) while doubling the trial rate compared to $2rm$ memories in [8].

For the proposed architecture we will mention below, we assume that the number of quantum emitters is not a concern and we care more about the ease of reasoning with the protocol and the generation process than optimizing the number of quantum emitters.

A. Functionally equivalent graph state to RGS

The complete graph connectivity of RGS in [5] is not a strict requirement in order to create a linear chain in the third stage mentioned in Sec. III-B. The only strict requirement to turn RGS into the linear chain graph state in the right image in Fig. 4 is that each first-leaf qubit in one half needs to be connected to all first-leaf qubits of the other half. This allows us to introduce RGS', shown in Fig. 6(d), a functionally equivalent graph state to RGS, where the first-leaf qubits form a complete bipartite graph $K_{m,m}$. We will refer to both RGS and RGS' as RGS when it is unnecessary to distinguish them as they both achieve the same tasks.

B. RGS' generation

The generation of RGS is the most difficult part in realizing the RGS scheme. Various generation methods have been proposed [5], [6], [38]–[42]. In this work, we use a modified version of the deterministic generation of RGS via quantum emitters analyzed in [7], [39].

We assume that the RGSS is equipped with quantum emitters arranged in a linear topology ($Q_0, Q_1, Q_2, \dots, Q_{n+1}$), and Hadamard gates can be applied on individual emitters, as well as controlled-phase gates CZ between neighboring ones.

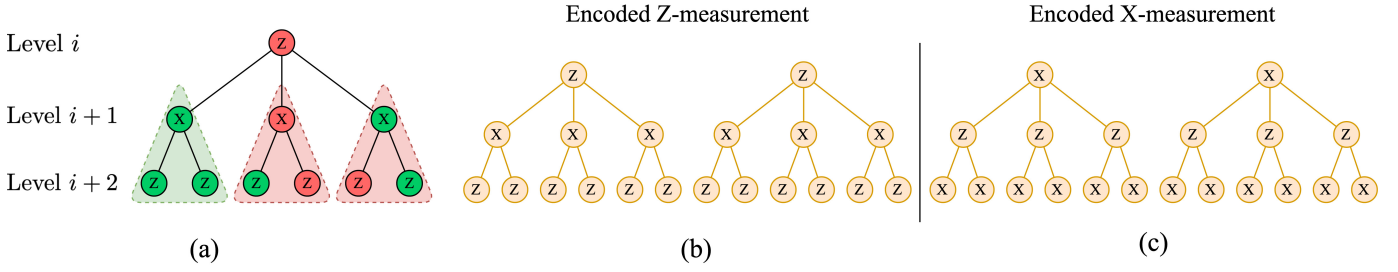


Fig. 5. (a) A successful indirect Z-measurement of a qubit at level- i even though the direct measurement failed (red vertex) due to lost and even with middle and right subtree failed. (b), (c) Logical measurement on the encoded tree, letters inside the node refer to the basis of measurement.

Photon emission is modeled using controlled-not gate CX , as shown in Fig. 6(a).

In addition to the manipulation rules of graph state mentioned previously, we will need a *push-out operation*, where the emitter in the graph state is replaced with the newly emitted photon, and the emitter is now connected to only the new photon [43], [44]. This is achieved by photon emission followed by a Hadamard gate, as depicted in Fig. 6(b). The sequence of generating half-RGS with m arms with branching vector $\vec{b} = (b_0, b_1, \dots, b_{n-1})$ anchored at Q_0 on one side is given by (also depicted in Fig 6(c))

$$\begin{aligned}
 & (M_{X,Q_1} M_{X,Q_2} CZ_{Q_0,Q_1} CZ_{Q_1,Q_2} G_0 E_{\text{ph},Q_1})^m \\
 & \text{with } G_k = M_{Z,Q_{k+2}} H_{Q_{k+2}} E_{\text{ph},Q_{k+2}} CZ_{Q_{k+1},Q_{k+2}} G_{k+1}^{b_k} \\
 & \text{and } G_{n-1} = E_{\text{ph},Q_{n+1}},
 \end{aligned} \tag{11}$$

where E_{ph,Q_i} and M_{B,Q_i} denotes photon emission and measurement in the B basis on emitter i respectively. The final step in creating RGS' is to perform CZ between Q_0 on the left and right side and perform the XX -measurement.

Single-qubit rotations of photonic qubits are left out for simplicity. We will come back to address them in Sec. V when we discuss fixing local Clifford (VOP) effects.

C. End nodes

Now that we have split the RGS generation into two separate parts, we can see that the half-RGS which is the intermediate state shown in Fig. 6 at RGSS, can also be used at end nodes. This allows end nodes to use the same implementations as RGSSs while reducing the number of memories from rm to only m emitters. Instead of joining the two Q_0 anchors of the left and right side creating RGS', since end nodes only require one half-RGS, end nodes can swap the anchor qubit Q_0 to a longer-lifetime memory qubit. The number of memories required to keep up with the trial rate is r instead of rm and the repetition rate is also doubled compared to RGSS having a single set of emitters generating RGS as well. This realization enables smooth integration of end nodes into the RGS scheme, which has been neglected in most related research.

D. Timing signals

The original RGS scheme requires that the second-leaf qubits from both sides arrive at the ABSA nearly at the

same time, within an indistinguishable time window, for the entanglement swapping via BSM to work. Since we separate the two halves of RGS' to be generated by a different set of emitters, the timing message only needs to be exchanged between neighbors and the controller which controls the emitter at each link in the same way as for conventional memory-based repeaters. This is unlike the case where the whole graph is generated by one set of emitters [7]. In the single-set case, the timing message must be sent to both left and right nodes to achieve the required coordination along the entire connection path, a significant complication in engineering that our scheme avoids.

E. Advanced Bell state analyzer (ABSA)

We assume that the BSM device at ABSA measures the Bell pair in the usual Bell basis and it can only distinguish between

$$|\Psi^\pm\rangle = (|01\rangle \pm |10\rangle)/\sqrt{2}, \tag{12}$$

and cannot distinguish between the remaining two Bell states,

$$|\Phi^\pm\rangle = (|00\rangle \pm |11\rangle)/\sqrt{2}. \tag{13}$$

Although in the RGS scheme, the BSM is usually described as a rotated Bell basis, we will show in Sec. V that we can also use the conventional Bell basis. This is desirable from an implementation point of view. It means that one does not need to build special detectors for the RGS scheme as normal components from memory-based schemes are sufficient.

We also make an assumption here that the interval between each physical qubit of first-leaf qubits arriving at ABSA is long enough that the change of measurement basis between X and Z can be performed without any issues.

F. Integration into memory-based architecture

Our architecture fits well within the framework of RuleSet-based protocols proposed in [22], [34]. The traditional RGS scheme has been introduced as an alternative to conventional memory-based repeaters. This view may be appropriate in the context of QKD applications but requires reconsideration if the desired distributed states are correctable Bell pairs. In light of our current discussion, it is more appropriate to consider the RGS scheme as a link-level connection, as depicted in Fig. 7. This leads to far greater flexibility. In particular, the RGS scheme can be used to connect any two nodes, not

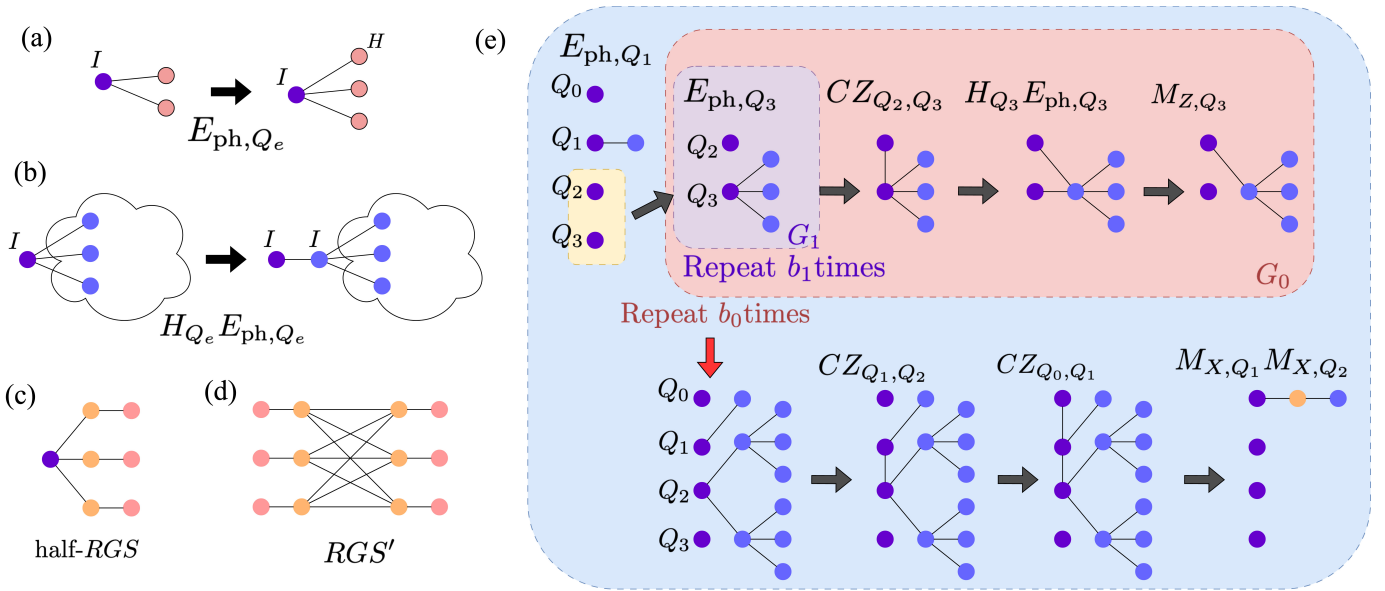


Fig. 6. (a) Emission of a photon with VOPs. (b) The push-out operation, photon emission followed by Hadamard, is shown with VOPs. (c) A half-RGS, a tree graph anchored at an emitter during RGS generation. (d) A functionally equivalent RGS. (e) The sequence (modified from [7]) to generate one arm of half-RGS with $\bar{b} = (2, 3)$. This needs to be repeated m times to create m arms.

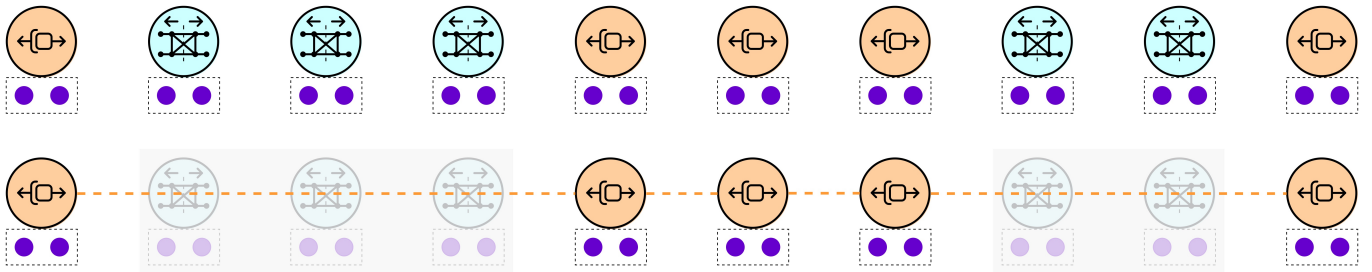


Fig. 7. Links constituting RGSS and ABSA (omitted) are treated as virtual links to memory-equipped repeaters (orange icons). The RGS scheme link is invisible at the connection level protocol.

necessarily only end nodes. The Bell pairs created from the RGS scheme at the link level can be treated the same way as link-level resources created from other link architectures, such as Meet-in-the-Middle, Memory-Memory [45], Memory-Source-Memory [46], or Sneakernet links [47], and later can be allocated to the resource management software of the quantum nodes. This is in the spirit of heterogeneity and interoperability of the future quantum internet [34].

V. CORRECTIONS TO MAINTAIN GRAPH STATE

Having covered our proposed architecture, we will now discuss how actual measurements are performed at the ABSA, and what information is required to be communicated to which nodes.

A. How VOPs affect measurement results

Recall that the three operations required to generate an RGS are photon emission, push-out operation, and measurement. For the emit operation (not the push-out), the newly created photon needs to be corrected via the Hadamard gate to remove

the VOP (H). We assume that the photonic Hadamard can be done at the RGSS nodes. On the other hand, the push-out operation does not need any correction since no VOP is introduced in this operation. However, the Z -measurement on emitters during the arm generation can create Z side effects on the photon qubits. Fortunately, this Z VOP on the photonic qubit which is part of first-leaf qubits, will only flip the results of X -measurements and does not change the result of the Z -measurement. This means that in order to correct the final end-to-end Bell pair, this information must be passed to either the ABSA or the end nodes in order to compute the correction needed.

For the XX -measurement at the last step of each arm, connecting second-leaf and first-leaf qubits and attaching the arm to the anchor qubit may also introduce Z corrections on both the logical first-leaf qubits and the second-leaf qubit. Z correction on first leaf qubits as mentioned before can be handled easily at the end nodes.

For second-leaf qubits, as we can see that the conventional BSM is just a rotated BSM (CZ followed by XX -

measurement) with an additional H gate in front (depicted in Fig. 8). This means that the RGSS on one side can send the emitted photons without correcting the H (VOP) as the H will be canceled on the bottom wire. When a Z VOP occurs on the second-leaf qubits, it means that the Bell state registered as a successful measurement at ABSA can turn from $|\Psi^\pm\rangle$ into $|\Phi^\pm\rangle$ but this can also be fixed at end nodes as long as we know the VOP from RGSS.

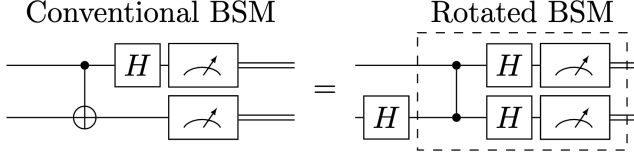


Fig. 8. Conventional Bell state measurement the rotated Bell measurement (dashed) circuits. Rotated BSM is often used in the measurement-based quantum computing and graph state literature. It can be seen that the conventional BSM is just a rotated-BSM with an additional Hadamard gate on one of the input qubits.

B. Amount of information needed for correction

It is clear that we need every measurement result performed at RGSSs and ABSAs to correct the final Bell pair. This means that for each trial, every RGSS and ABSA needs to send out b_{RGSS} and b_{ABSA} bits of information to the end nodes, where these values can be given by

$$b_{RGSS} = 2 + 2m \left(2 + \sum_{k=0}^{n-2} \prod_{j=0}^k b_j \right) \quad (14)$$

and

$$b_{ABSA} = 2m \left(2 + \sum_{k=0}^{n-1} \prod_{j=0}^k b_j \right), \quad (15)$$

where b_j refers to the branching factor at index j of vector \vec{b} .

Depending on the structure of the RGS, this can be quite a large amount of information that should be sent to get a single Bell pair. In fact, we can do better, by having each RGSS send their measurement result to the ABSA they are connected to, instead of directly to end nodes. The ABSA can then combine the information it receives and send just 2 bits of information to the end nodes.

VI. RGS PROTOCOL

In this section, we will outline the general idea of how one can implement the communication protocol to realize the RGS scheme with our proposed architecture. We will not go into the details of how the message should be structured but we will describe what information must be included and how each node uses this information to coordinate an end-to-end Bell pair for each trial.

We assume that the message exchanges between two end nodes (connection setup) are completed, thus the number of RGS arms m and the branching vectors \vec{b} are now known to all nodes along the connection path. We also assume that RGSS

and ABSA know the photon ordering and the time between each photon, given each setting of m and \vec{b} . Then for each trial, the tasks for ABSA and RGSS go as follows.

- 1) ABSA sends a notification message to its neighboring RGSSs about when the first photon should arrive.
- 2) RGSS emits the photonic RGS and keeps the measurement results during the generation process.
- 3) From the measurement results, RGSS constructs a correction tree for each logical first-leaf qubit.
- 4) RGSS sends the correction trees (to correct physical qubit measurements), logical correction (to flip the logical first-leaf result), and correction to the second-leaf qubit of each of the m arms in a single message.
- 5) ABSA decides if the trial is a success or a failure. If the trial is a failure, sends a failure message to end nodes. If not, ABSA proceeds to the next step.
- 6) ABSA constructs its measurement result tree from the measurement result of the coming photonic qubits for each logical qubit.
- 7) For each of the RGSS's message, ABSA merges the information of the correction tree and its own measurement result tree and computes the logical measurement result of each of the first-leaf qubit.
- 8) ABSA uses logical correction to decide if the first-leaf qubit result should be flipped or stay as is.
- 9) ABSA uses the second-leaf correction and the logical result to compute the correction at end nodes and sends a message to the end nodes, indicating that the trial is successful at this segment of the path and what Pauli correction should be done from this segment.

For the tree at an RGSS, each node is assigned a value of $+1$ or -1 when the emitter was measured in the Z basis after the push-out operation after getting $+1$ or -1 eigenvalue, respectively. At the ABSA, each node in this tree can be assigned a value of $+Z$, $-Z$, $+X$, $-X$ or L where $\pm Z$ and $\pm X$ corresponds to ± 1 result of Z -measurement and X -measurement, respectively, while L refers to photon being lost. The merge operation at the ABSA can be described as the following. The value of ± 1 from the RGSS's tree will flip $\pm X$ into $\mp X$ while not changing other values.

It should be noted that although a tree is not a naturally serial data structure, one can easily send the tree encoding of each logical qubit in either postorder traversal, preorder traversal, or level traversal of the tree in an array format. The index mapping of the tree, entry i of the array to the placement of node in the tree, can be figured out easily since the logical tree encoding has a well-defined branching vector \vec{b} and the tree is a complete tree thus a single tree traversal array suffices.

VII. DISCUSSION

We have introduced a concrete communication protocol that can be used to implement the all-photonic RGS scheme proposed in [5], and an architecture to support the proposed protocols. All-photonic repeaters have so far been investigated in the context of QKD applications only. Our work generalizes the scheme to applications that require a corrected Bell pair

as the final resource by including end nodes in the protocol and the architecture. This allows us to smoothly integrate our approach into the conventional memory-based repeater networks that support the architecture proposed in [34]. This allows us to treat the RGS scheme as a virtual physical link at the same level as existing memory-based link architectures.

Sending information about all the measurement outcomes to the end nodes in order to compute the correction operations requires an enormous amount of information to be processed. Our proposed protocol avoids this problem by determining the correction operations in two phases. First, each ABSA determines the required correction, and then it takes the necessary actions to correct the state. This way, only two bits of information are required to be sent from each ABSA to the end nodes informing them of the success of these local corrections.

Another underexplored area regarding the RGS scheme is its robustness against complex noise models. Such models are not amenable to analytic studies and require simulation. Most quantum network simulators [22], [48], [49] are built for simulating memory-based repeaters. These simulators are capable of handling hundreds of thousands of qubits in the system. However, the qubits only form small-sized entangled states, each comprising between 2-10 qubits. Since the RGS scheme's core idea is based on highly entangled states of hundreds if not thousands of qubits, simulators capable of simulating the RGS scheme with non-Pauli noise would require Monte Carlo methods or shot-based simulation to gather statistics. One possible way to simulate the RGS scheme is to utilize the error basis model mentioned in [22] by extending this to be applied on decorated graph states and not just based on bipartite Bell states. Combining the error basis model with stabilizer simulations [26], [50], [51] would be the straightforward way to achieve this generalization. However, it should be noted that only Anders' graph state simulator [26] allows adding and removing qubits during the simulation without much penalty. A different approach is to utilize the noisy stabilizer formalism [52] and integrate classical message delay into it.

It should be noted that although the RGS scheme can also be tolerant to quantum operational errors via a majority vote during the indirect Z -measurements of the logical first-leaf qubits, we have not included that into our protocol and we defer it to future work. Other possible research directions include extending our protocol to the distribution of multipartite states such as the GHZ state. The half-RGS generation method used in our architecture lends itself naturally for this purpose. Detailed analysis of the generation time, and the performance evaluation of mixed RGS and memory-based architecture versus RGS-only and memory-only architectures, remains a pressing open question.

REFERENCES

- [1] H.-J. Briegel, W. Dür, J. I. Cirac, and P. Zoller, "Quantum Repeaters: The Role of Imperfect Local Operations in Quantum Communication," *Physical Review Letters*, vol. 81, no. 26, pp. 5932–5935, Dec. 1998. doi:10.1103/PhysRevLett.81.5932
- [2] W. Dür, H.-J. Briegel, J. I. Cirac, and P. Zoller, "Quantum repeaters based on entanglement purification," *Physical Review A*, vol. 59, no. 1, pp. 169–181, Jan. 1999. doi:10.1103/PhysRevA.59.169
- [3] S. Wehner, D. Elkouss, and R. Hanson, "Quantum internet: A vision for the road ahead," *Science*, vol. 362, no. 6412, p. eaam9288, 2018. doi:10.1126/science.aam9288
- [4] W. Kozłowski *et al.*, "Architectural Principles for a Quantum Internet," RFC 9340, Mar. 2023. doi:10.17487/RFC9340
- [5] K. Azuma, K. Tamaki, and H.-K. Lo, "All-photonic quantum repeaters," *Nature Communications*, vol. 6, no. 1, p. 6787, Apr. 2015. doi:10.1038/ncomms7787
- [6] M. Pant, H. Krovi, D. Englund, and S. Guha, "Rate-distance tradeoff and resource costs for all-optical quantum repeaters," *Physical Review A*, vol. 95, no. 1, p. 012304, Jan. 2017. doi:10.1103/PhysRevA.95.012304
- [7] P. Hilaire, E. Barnes, and S. E. Economou, "Resource requirements for efficient quantum communication using all-photonic graph states generated from a few matter qubits," *Quantum*, vol. 5, p. 397, Feb. 2021. doi:10.22331/q-2021-02-15-397
- [8] Y. Zhan, P. Hilaire, E. Barnes, S. E. Economou, and S. Sun, "Performance analysis of quantum repeaters enabled by deterministically generated photonic graph states," *Quantum*, vol. 7, p. 924, Feb. 2023. doi:10.22331/q-2023-02-16-924
- [9] C. H. Bennett, G. Brassard, C. Crépeau, R. Jozsa, A. Peres, and W. K. Wootters, "Teleporting an unknown quantum state via dual classical and einstein-podolsky-rosen channels," *Phys. Rev. Lett.*, vol. 70, pp. 1895–1899, Mar 1993. doi:10.1103/PhysRevLett.70.1895
- [10] A. K. Ekert, "Quantum cryptography based on bell's theorem," *Phys. Rev. Lett.*, vol. 67, pp. 661–663, Aug 1991. doi:10.1103/PhysRevLett.67.661
- [11] C. H. Bennett, G. Brassard, and N. D. Mermin, "Quantum cryptography without bell's theorem," *Phys. Rev. Lett.*, vol. 68, pp. 557–559, Feb 1992. doi:10.1103/PhysRevLett.68.557
- [12] D. Gottesman, T. Jennewein, and S. Croke, "Longer-baseline telescopes using quantum repeaters," *Phys. Rev. Lett.*, vol. 109, p. 070503, Aug 2012. doi:10.1103/PhysRevLett.109.070503
- [13] J.-P. Chen *et al.*, "Quantum key distribution over 658 km fiber with distributed vibration sensing," *Phys. Rev. Lett.*, vol. 128, p. 180502, May 2022. doi:10.1103/PhysRevLett.128.180502
- [14] A. Broadbent, J. Fitzsimons, and E. Kashefi, "Universal blind quantum computation," in *2009 50th Annual IEEE Symposium on Foundations of Computer Science*, 2009, pp. 517–526. doi:10.1109/FOCS.2009.36
- [15] J. F. Fitzsimons and E. Kashefi, "Unconditionally verifiable blind quantum computation," *Phys. Rev. A*, vol. 96, p. 012303, Jul 2017. doi:10.1103/PhysRevA.96.012303
- [16] M. Hayashi and M. Hajdušek, "Self-guaranteed measurement-based quantum computation," *Phys. Rev. A*, vol. 97, p. 052308, May 2018. doi:10.1103/PhysRevA.97.052308
- [17] R. Van Meter, "Architecture of a quantum multicompiler optimized for Shor's factoring algorithm," PhD thesis, Keio University, 2006. doi:10.48550/arXiv.quant-ph/0607065
- [18] D. Cuomo, M. Caleffi, and A. S. Cacciapuoti, "Towards a distributed quantum computing ecosystem," *IET Quantum Communication*, vol. 1, no. 1, pp. 3–8, 2020. doi:10.1049/iet-qt.2020.0002
- [19] M. Ben-Or and A. Hassidim, "Fast quantum byzantine agreement," in *Proceedings of the Thirty-Seventh Annual ACM Symposium on Theory of Computing*, 2005, p. 481–485. doi:10.1145/1060590.1060662
- [20] C. Meignant, D. Markham, and F. Grosshans, "Distributing Graph States Over Arbitrary Quantum Networks," *Physical Review A*, vol. 100, no. 5, p. 052333, Nov. 2019. doi:10.1103/PhysRevA.100.052333
- [21] A. Fischer and D. Towsley, "Distributing graph states across quantum networks," in *2021 IEEE International Conference on Quantum Computing and Engineering (QCE)*, 2021, pp. 324–333. doi:10.1109/QCE52317.2021.00049
- [22] R. Satoh *et al.*, "Quisp: a quantum internet simulation package," in *2022 IEEE International Conference on Quantum Computing and Engineering (QCE)*. Broomfield, CO, USA: IEEE, Sep 2022, p. 353–364. doi:10.1109/QCE53715.2022.00056
- [23] M. Hein, J. Eisert, and H. J. Briegel, "Multiparty entanglement in graph states," *Physical Review A*, vol. 69, no. 6, p. 062311, Jun. 2004. doi:10.1103/PhysRevA.69.062311
- [24] M. Hein, W. Dür, J. Eisert, R. Raussendorf, M. V. den Nest, and H.-J. Briegel, "Entanglement in Graph States and its Applications," *arXiv:quant-ph/0602096*, Feb. 2006. doi:10.48550/arXiv.quant-ph/0602096

- [25] D. E. Gottesman, “Stabilizer codes and quantum error correction,” Ph.D. dissertation, California Institute of Technology, Jul 2004. doi:10.7907/RZR7-DT72
- [26] S. Anders and H. J. Briegel, “Fast simulation of stabilizer circuits using a graph-state representation,” *Phys. Rev. A*, vol. 73, p. 022334, Feb 2006. doi:10.1103/PhysRevA.73.022334
- [27] M. Van den Nest, J. Dehaene, and B. De Moor, “Graphical description of the action of local clifford transformations on graph states,” *Phys. Rev. A*, vol. 69, p. 022316, Feb 2004. doi:10.1103/PhysRevA.69.022316
- [28] M. Grassl, A. Klappenecker, and M. Rotteler, “Graphs, quadratic forms, and quantum codes,” in *Proceedings IEEE International Symposium on Information Theory*, 2002, p. 45. doi:10.1109/ISIT.2002.1023317
- [29] D. Schlingemann, “Stabilizer codes can be realized as graph codes,” *Quantum Info. Comput.*, vol. 2, no. 4, p. 307–323, jun 2002. doi:10.48550/arXiv.quant-ph/0111080
- [30] M. Zwerger, W. Dür, and H. J. Briegel, “Measurement-based quantum repeaters,” *Physical Review A*, vol. 85, no. 6, p. 062326, Jun. 2012. doi:10.1103/PhysRevA.85.062326
- [31] M. Zwerger, H. J. Briegel, and W. Dür, “Measurement-based quantum communication,” *Applied Physics B*, vol. 122, no. 3, p. 50, Mar 2016. doi:10.1007/s00340-015-6285-8
- [32] J. Borregaard, H. Pichler, T. Schröder, M. D. Lukin, P. Lodahl, and A. S. Sørensen, “One-Way Quantum Repeater Based on Near-Deterministic Photon-Emitter Interfaces,” *Physical Review X*, vol. 10, no. 2, p. 021071, Jun. 2020. doi:10.1103/PhysRevX.10.021071
- [33] M. Varnava, D. E. Browne, and T. Rudolph, “Loss Tolerance in One-Way Quantum Computation via Counterfactual Error Correction,” *Physical Review Letters*, vol. 97, no. 12, p. 120501, Sep. 2006. doi:10.1103/PhysRevLett.97.120501
- [34] R. Van Meter *et al.*, “A Quantum Internet Architecture,” in *2022 IEEE International Conference on Quantum Computing and Engineering (QCE)*. Broomfield, CO, USA: IEEE, Sep. 2022, pp. 341–352. doi:10.1109/QCE53715.2022.00055
- [35] M. Żukowski, A. Zeilinger, M. A. Horne, and A. K. Ekert, ““event-ready-detectors” bell experiment via entanglement swapping,” *Phys. Rev. Lett.*, vol. 71, pp. 4287–4290, Dec 1993. doi:10.1103/PhysRevLett.71.4287
- [36] Y. Hasegawa *et al.*, “Experimental time-reversed adaptive Bell measurement towards all-photon quantum repeaters,” *Nature Communications*, vol. 10, no. 1, p. 378, Jan. 2019. doi:10.1038/s41467-018-08099-5
- [37] Z.-D. Li *et al.*, “Experimental quantum repeater without quantum memory,” *Nature Photonics*, vol. 13, no. 9, pp. 644–648, Sep. 2019. doi:10.1038/s41566-019-0468-5
- [38] Y. Zhan and S. Sun, “Deterministic Generation of Loss-Tolerant Photonic Cluster States with a Single Quantum Emitter,” *Physical Review Letters*, vol. 125, no. 22, p. 223601, Nov. 2020. doi:10.1103/PhysRevLett.125.223601
- [39] D. Buterakos, E. Barnes, and S. E. Economou, “Deterministic Generation of All-Photonic Quantum Repeaters from Solid-State Emitters,” *Physical Review X*, vol. 7, no. 4, p. 041023, Oct. 2017. doi:10.1103/PhysRevX.7.041023
- [40] P. Hilaire, L. Vidro, H. S. Eisenberg, and S. E. Economou, “Near-deterministic hybrid generation of arbitrary photonic graph states using a single quantum emitter and linear optics,” May 2022. doi:10.48550/arXiv.2205.09750
- [41] B. Li, S. E. Economou, and E. Barnes, “Photonic resource state generation from a minimal number of quantum emitters,” *npj Quantum Information*, vol. 8, no. 1, pp. 1–7, Feb. 2022. doi:10.1038/s41534-022-00522-6
- [42] H. Shapourian and A. Shabani, “Modular architectures to deterministically generate graph states,” *Quantum*, vol. 7, p. 935, Mar 2023. doi:10.22331/q-2023-03-02-935
- [43] S. E. Economou, N. Lindner, and T. Rudolph, “Optically Generated 2-Dimensional Photonic Cluster State from Coupled Quantum Dots,” *Physical Review Letters*, vol. 105, no. 9, p. 093601, Aug. 2010. doi:10.1103/PhysRevLett.105.093601
- [44] A. Russo, E. Barnes, and S. E. Economou, “Generation of arbitrary all-photon graph states from quantum emitters,” *New Journal of Physics*, vol. 21, no. 5, p. 055002, May 2019. doi:10.1088/1367-2630/ab193d
- [45] N. Sangouard, C. Simon, H. De Riedmatten, and N. Gisin, “Quantum repeaters based on atomic ensembles and linear optics,” *Reviews of Modern Physics*, vol. 83, no. 1, pp. 33–80, Mar. 2011. doi:10.1103/RevModPhys.83.33
- [46] C. Jones, D. Kim, M. T. Rakher, P. G. Kwiat, and T. D. Ladd, “Design and analysis of communication protocols for quantum repeater networks,” *New Journal of Physics*, vol. 18, no. 8, p. 083015, Aug. 2016. doi:10.1088/1367-2630/18/8/083015
- [47] S. J. Devitt, A. D. Greentree, A. M. Stephens, and R. Van Meter, “High-speed quantum networking by ship,” *Scientific Reports*, vol. 6, no. 1, p. 36163, Nov. 2016. doi:10.1038/srep36163
- [48] X. Wu *et al.*, “Sequence: a customizable discrete-event simulator of quantum networks,” *Quantum Science and Technology*, vol. 6, no. 4, p. 045027, 2021. doi:10.1088/2058-9565/ac22f6
- [49] T. Coopmans *et al.*, “Netsquid, a network simulator for quantum information using discrete events,” *Communications Physics*, vol. 4, no. 1, p. 164, 2021. doi:10.1038/s42005-021-00647-8
- [50] S. Aaronson and D. Gottesman, “Improved simulation of stabilizer circuits,” *Physical Review A*, vol. 70, no. 5, p. 052328, Nov. 2004. doi:10.1103/PhysRevA.70.052328
- [51] C. Gidney, “Stim: A fast stabilizer circuit simulator,” *Quantum*, vol. 5, p. 497, Jul. 2021. doi:10.22331/q-2021-07-06-497
- [52] M. F. Mor-Ruiz and W. Dür, “Noisy Stabilizer Formalism,” Dec. 2022. doi:10.48550/arXiv.2212.08677